

# Determination of uncertainty profiles in neutral atmospheric properties measured by radio occultation experiments

A. Bourgoïn,<sup>1,2</sup> E. Gramigna,<sup>3</sup> M. Zannoni,<sup>3,4</sup> L. Gomez Casajus,<sup>4</sup> and P. Tortora<sup>3,4</sup>

<sup>1</sup>*SYRTE, Observatoire de Paris, PSL Research University, CNRS, Sorbonne Universités, UPMC P6, LNE, 61 avenue de l'Observatoire, 75014 Paris, France*

<sup>2</sup>*Département d'Astrophysique-AIM, CEA/DRF/IRFU, CNRS/INSU,*

*Université Paris-Saclay, Université de Paris, 91191 Gif-sur-Yvette, France\**

<sup>3</sup>*Dipartimento di Ingegneria Industriale, Alma Mater Studiorum – Università di Bologna, Via Fontanelle 40, 47121 Forlì, Italy*

<sup>4</sup>*Centro Interdipartimentale di Ricerca Industriale Aerospaziale (CIRI AERO), Alma Mater Studiorum – Università di Bologna, Via Baldassarre Carnaccini 12, 47121 Forlì, Italy*

(Dated: 19 octobre 2021)

Radio occultations are commonly used to assess remotely atmospheric properties of planets or satellites within the solar system. The data processing usually involves the so-called Abel inversion method or the numerical ray-tracing technique. Both are now well established, however, they do not allow to easily determine the uncertainty profiles in atmospheric properties, and this makes results difficult to interpret statistically. Recently, a purely analytical approach based on the time transfer functions formalism was proposed for modeling radio occultation data. Using this formulation, we derive uncertainty relationships between the frequency shift and neutral atmosphere properties such as temperature, pressure, and neutral number density. These expressions are relevant for interpreting previous results from past radio occultation experiments and for deriving the system requirements for future missions in a rigorous manner, and consistently with the scientific requirements about the atmospheric properties retrieval.

## I. INTRODUCTION

When an electromagnetic signal crosses an optical medium it experiences refraction. Refraction operates at two different levels within the framework of geometrical optics. First, it causes the phase of the signal to slow down or speed up while propagating in a neutral or ionized medium, respectively. Secondly, it bends the signal towards regions of higher index of refraction. Both effects introduce delays and hence frequency shifts with respect to a signal that would have been transmitted in a vacuum.

Occultation experiments precisely exploit refraction in order to remotely retrieve the atmospheric properties of planetary atmospheres (i.e., ionosphere and neutral atmosphere). The basic principle is to establish an electromagnetic link between two separated elements when a planetary atmosphere stands between them. Accordingly, the electromagnetic signal is affected by the presence of the atmosphere and experiences perturbations with respect to a signal that would have been transmitted in a vacuum (i.e., in the absence of the atmosphere). By analyzing these perturbations one can retrieve the atmospheric properties of the occulting atmosphere. If the element that transmits the signal is a distant star, the experiment is called a “stellar occultation” (see e.g., Roques *et al.* [1], Sicardy *et al.* [2]) while it is called a “radio occultation” if the transmitting element is a spacecraft radio system (see e.g., Kliore *et al.* [3], Fjeldbo and Eshleman [4, 5], Lindal *et al.* [6, 7], Lindal [8], Schinder *et al.* [9, 10]). Within this last category, if the receiving element is also located on a spacecraft, the radio occultation experiment is a “spacecraft-spacecraft” experiment (see e.g., GPS/MET experiment [11] or GPS/COSMIC [12] experiment), whereas it is called a “spacecraft-Earth” experiment if the receiving element is located on Earth (see e.g., Phinney and Anderson [13], Fjeldbo *et al.* [14]). In this paper, we focus on radio occultations in a spacecraft-Earth configuration.

Two methods are commonly employed for processing radio occultations data, namely the “Abel inversion” [13] and the “numerical ray-tracing” [10]. The Abel inversion is employed when the occulting atmosphere can be assumed to be spherically symmetric. It is an exact expression providing the index of refraction profile directly from the bending angle which is the angle between the direction of the ray path before entering the atmosphere and the direction of the ray path after exiting the atmosphere. The bending angle is itself retrieved from the frequency shift due to the presence of the atmosphere along the light path. The ray-tracing method consists in a numerical integration of the equations describing the optical rays across a layered barotropic atmosphere. The refractivity in each layer and the direction of the ray path before it entered the atmosphere are iteratively determined such that the computed

---

\* adrien.bourgoïn@obspm.fr

frequency matches the observed frequency. Although the ray-tracing method is the most general one, it requires a very significant computational time.

Regarding statistical errors, both the Abel inversion and the ray-tracing do not allow to easily associate uncertainty profiles to the atmospheric properties that are derived. This makes the results of past radio occultation experiments and the preliminary design of future experiments difficult to interpret statistically. To overcome this issue, Withers [15] derived simple relationships relating the frequency shift uncertainty to the electron density and neutral number density uncertainties. The method assumes vertical exponential profiles for both the ionosphere and the neutral atmosphere and then exploits the integral form of the Abel transform to derive the relationships. The derived uncertainty profiles are thus dependent on the scale heights of both ionosphere and neutral atmosphere. In a revised version, Withers [16] proposed an alternative approach that do not require an *a priori* knowledge of the scale heights. This revised formulation, based on the Abel transform too, only depends on the vertical resolution. While in principle it could be employed to perform preliminary design of future radio occultation experiments, it still remains challenging to predict changes in the vertical resolution at the ground level without an *a priori* knowledge of the scale heights. Schinder *et al.* [17] proposed a purely numerical approach based on Monte-Carlo simulations. This method allows to directly derive the uncertainty profiles on the final outputs, namely the temperature and pressure profiles. Although it is well suited to interpret results from past radio occultation experiments, it cannot be directly applied to perform preliminary design of future radio occultation experiments. Finally, we mention the work by Lipa and Tyler [18] who developed a sophisticated method of propagation of errors. The method is well suited for a numerical resolution algorithm but it cannot be directly applied to the design future experiments. In that sense, the analytical methods proposed by Withers [15, 16] are more convenient than purely numerical methods.

Recently, it was shown by Bourgoïn [19], that in the context of relativistic geometrical optics, the time and frequency transfers can be analytically determined up to the appropriate order while considering both the effects of gravity and refraction due to a neutral medium. The relativistic counterpart for ionized medium is challenging to elaborate within a covariant formalism, therefore the present paper focuses on neutral medium only. The approach by Bourgoïn [19] is based on two theoretical tools, namely the time transfer functions formalism [20, 21] and the optical metric of spacetime [22], also called Gordon's metric. The latter allows to handle refraction caused by neutral medium as spacetime curvature while the former handles theoretical problems related to the time and frequency transfers in curved spacetime. The formalism introduced by Bourgoïn [19] was used recently by Bourgoïn *et al.* [23] for modeling the time and frequency transfers in radio occultation experiments. The authors derived the first order expressions of the time and frequency transfers due to a spherically symmetric atmosphere considering the relativistic light-dragging effect. This relativistic effect is naturally accounted for by the covariant formalism and represents in that sense a significant improvement with respect to previous perturbation approaches within the framework of non-relativistic geometrical optics [24]. From the analytical solutions derived in Bourgoïn *et al.* [23] it is possible to derive the uncertainty relationships between the frequency shift and the physical properties of the neutral atmosphere, such as neutral number density, temperature, and pressure as functions of the altitude. This is precisely the aim of the present paper.

The paper is organized as follows. Section II lists the notations and assumptions we make throughout the paper. Section III recalls the main results of Bourgoïn [19] concerning the formalism of time transfer functions applied to the propagation of light across neutral medium. Section IV recalls the main results of Bourgoïn *et al.* [23] concerning the application of the time transfer functions formalism to radio occultation experiments when the occulting atmosphere is spherically symmetric. The solutions are simplified, assuming an isothermal profile across the atmosphere and neglecting the relativistic light-dragging effect. In Sect. V, the uncertainty relationships in atmospheric properties are derived and applied to results of past radio occultation experiments. The outputs are also compared to predictions by Withers [15] and Withers [16]. Finally, we give our conclusions in Sect. VI.

## II. GENERAL ASSUMPTIONS AND NOTATIONS

This paper focuses on the propagation of light rays through a linear, isotropic, and nondispersive medium filling a spatially bounded region of spacetime  $\mathcal{D}$ . The regions of spacetime outside  $\mathcal{D}$  are supposed to be empty of any matter. The domain  $\mathcal{D}$  represents the limit of the neutral atmosphere.

The influence of gravity on the propagation of light is considered as negligible, so  $g$ , the physical metric of spacetime, is assumed to be a Minkowski metric. We systematically make use of an orthonormal Cartesian coordinate system  $(x^\mu) = (x^0, \mathbf{x})$ , so the components of the physical metric may be written such as

$$g_{\mu\nu} = \eta_{\mu\nu} = \text{diag}(+1, -1, -1, -1), \quad (1)$$

where Greek indices run from 0 to 3.

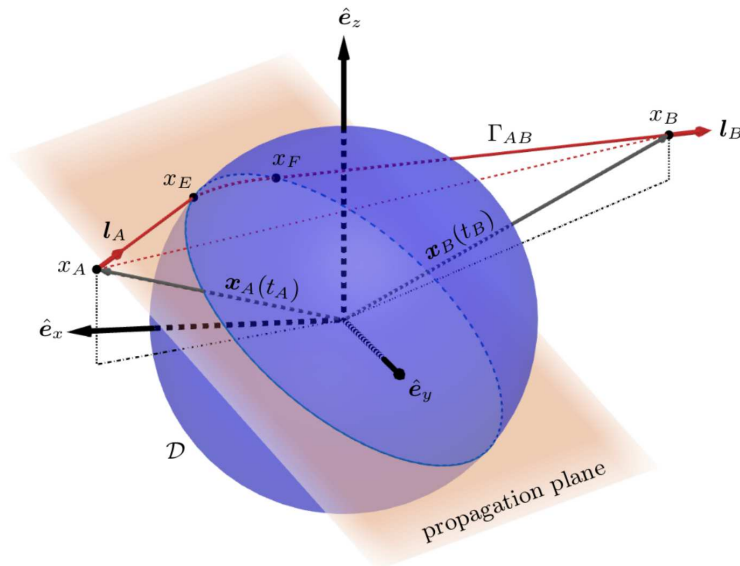


FIGURE 1. Schematic illustration of a radio occultation experiment. The vectorial basis  $(\hat{e}_x, \hat{e}_y, \hat{e}_z)$  is centered at the occulting body center-of-mass and is non-rotating with respect to distant stars. The light-ray  $\Gamma_{AB}$  is emitted at the point-event  $x_A$  with spatial coordinates  $\mathbf{x}_A(t_A)$ , and is received at  $x_B$  with spatial coordinates  $\mathbf{x}_B(t_B)$ . The point-events  $x_E$  and  $x_F$  are the atmosphere's entrance and exit points, respectively. The directions  $\mathbf{l}_A$  and  $\mathbf{l}_B$  are the unit-vectors that are tangent to  $\Gamma_{AB}$  at  $x_A$  and  $x_B$ , respectively. According to Eq. (1), they are given by  $\mathbf{l}_A = -\hat{\mathbf{L}}_A$  and  $\mathbf{l}_B = -\hat{\mathbf{L}}_B$ , respectively. For an occultation by a spherically symmetric atmosphere the propagation plane is fixed and contained the four point-events  $x_A$ ,  $x_E$ ,  $x_F$ , and  $x_B$ . The red dashed line joining  $x_A$  and  $x_B$  is the zeroth-order light-path lying on the surface of the past-light cone of  $x_B$  (see also figure 1 of Bourgoïn *et al.* [23] to appreciate the geometry of the occultation in a spacetime diagram).

We set  $x^0 = ct$ , with  $c$  being the speed of light in a vacuum and  $t$  a time coordinate, and we denote by  $\mathbf{x}$  the triple of spatial coordinates  $(x^1, x^2, x^3)$ . More generally, we use the notation  $\mathbf{a} = (a^1, a^2, a^3)$  for a triple constituted by the spatial components of a 4-vector and  $\underline{\mathbf{b}} = (b_1, b_2, b_3)$  for a triple built with the spatial components of a covariant 4-vector. According to assumption (1), we have  $\mathbf{b} = -\underline{\mathbf{b}}$ .

Given the triples  $\mathbf{a}$ ,  $\underline{\mathbf{b}}$ , and  $\mathbf{c}$ , the usual Euclidean scalar product  $\mathbf{a} \cdot \mathbf{c}$  is denoted by  $\sum_{i=1,3} a^i c^i$  and  $\mathbf{a} \cdot \underline{\mathbf{b}}$  denotes the quantity  $\sum_{i=1,3} a^i b_i$ . Furthermore, the Euclidean norm of  $\mathbf{a}$  and  $\underline{\mathbf{b}}$  are denoted by  $\|\mathbf{a}\| = (\mathbf{a} \cdot \mathbf{a})^{1/2}$  and  $\|\underline{\mathbf{b}}\| = (\underline{\mathbf{b}} \cdot \underline{\mathbf{b}})^{1/2}$ , respectively.

For the sake of legibility, we employ  $(f)_x$  or  $[f]_x$  instead of  $f(x)$  whenever necessary. When a quantity  $f(x)$  is evaluated at two point-events  $x_A$  and  $x_B$ , we employ  $f_{A/B}$  or  $(f)_{A/B}$  to denote  $f(x_A)$  and  $f(x_B)$ , respectively. The partial differentiations of  $f$  with respect to  $\mathbf{x}_A$  and  $\mathbf{x}_B$  are denoted by  $\partial_A f$  and  $\partial_B f$ , respectively. By definition,  $\partial_A$  and  $\partial_B$  are covariant triples and are always identified as such, hence, we omit the ‘‘underbar’’ for readability.

### III. TIME AND FREQUENCY TRANSFERS IN NEUTRAL MEDIUM

In this section, the main results from Bourgoïn [19] are recalled and the basic relations of the present paper are inferred by substituting the metric components  $g_{\mu\nu}$  from Eq. (1) into the equations provided into Bourgoïn [19]. In addition, a stationary spherically symmetric optical spacetime is assumed.

#### A. Time transfer function formalism

Let us consider a one-way transfer where a light ray  $\Gamma_{AB}$  is starting from an emission point-event  $x_A$  of coordinates  $(ct_A, \mathbf{x}_A)$  and arriving at a reception point-event  $x_B$  of coordinates  $(ct_B, \mathbf{x}_B)$ . We suppose that a part of  $\Gamma_{AB}$  travels through the domain  $\mathcal{D}$ , while the other part travels through a vacuum, that is to say a medium such that  $n = 1$  with  $n$  being the index of refraction. The geometry of the occultation is depicted in figure 1.

According to Bourgoïn *et al.* [23], within the geometrical optics framework, the eikonal function of an electromagnetic signal passing through a neutral medium, is a first integral along  $\Gamma_{AB}$  (this would no longer be the case for a ionized

medium which is part of the reason why formulating a covariant theory of light propagation into dispersive medium is challenging). This shows that  $t_A$  is an implicit function of  $\mathbf{x}_A$ ,  $t_B$ , and  $\mathbf{x}_B$ . Hence, it is appropriate to introduce  $\mathcal{T}$ , the reception time transfer function associated with  $\Gamma_{AB}$ , such as

$$t_B - t_A = \mathcal{T}(\mathbf{x}_A, t_B, \mathbf{x}_B). \quad (2)$$

For the simple case of a ray of light propagating in a vacuum without gravity effects (see assumption (1)), the time transfer function is simply given by  $\mathcal{T}(\mathbf{x}_A, \mathbf{x}_B) = \|\mathbf{x}_B - \mathbf{x}_A\|/c$ . However, in general, when the light ray propagates through the neutral medium contained into  $\mathcal{D}$ , the time transfer function is a much more complex expression.

Let  $k_\mu(x)$  be the 4-wave covector of the electromagnetic wave at  $x$ . An important quantity of the time transfer functions formalism is given by the covector  $\underline{\mathbf{l}}$  which is defined from the components  $k_\mu = (k_0, \underline{\mathbf{k}})$ . At the level of the emission and reception point-events, it is defined such as

$$\underline{\mathbf{l}}_{A/B} = \left( \frac{\underline{\mathbf{k}}}{k_0} \right)_{A/B}. \quad (3)$$

Then, according to Bourgoïn [19], the following useful expressions can be stated

$$\underline{\mathbf{l}}_A = \partial_A (c\mathcal{T}), \quad (4a)$$

$$\underline{\mathbf{l}}_B = - \left( 1 - \frac{\partial \mathcal{T}}{\partial t_B} \right)^{-1} \partial_B (c\mathcal{T}), \quad (4b)$$

$$\frac{(k_0)_B}{(k_0)_A} = 1 - \frac{\partial \mathcal{T}}{\partial t_B}. \quad (4c)$$

They are exact within the approximation of geometrical optics and they account for the effect of the refractive medium on the optical ray when it propagates into  $\mathcal{D}$ .

At the same approximation (i.e., the geometrical optics framework), the frequency transfer between the emitter and the receiver is exactly given by the following relationship (see e.g., Synge [25], Blanchet *et al.* [26]) :

$$\frac{\nu_B}{\nu_A} = \frac{(u^0 k_0)_B}{(u^0 k_0)_A} \left( \frac{1 + \beta_B \cdot \underline{\mathbf{l}}_B}{1 + \beta_A \cdot \underline{\mathbf{l}}_A} \right), \quad (5)$$

where  $\nu_A$  and  $\nu_B$  are the emitted and received frequencies, respectively,  $(u^0)_A$  and  $(u^0)_B$  are the time component of  $(u^\mu)_A$  and  $(u^\mu)_B$ , the unit 4-velocities of the emitter and receiver, respectively. The 4-velocities are by definition unit vectors for the physical metric of spacetime, hence, according to Eq. (1), we have the following relationship

$$(u^0)_{A/B} = \left( \frac{1}{\sqrt{1 - \|\beta\|^2}} \right)_{A/B}, \quad (6)$$

where  $\beta_A$  and  $\beta_B$  denote the coordinate 3-velocity vectors, namely

$$\beta_{A/B} = \left( \frac{\mathbf{u}}{u^0} \right)_{A/B} = \frac{1}{c} \left( \frac{d\mathbf{x}}{dt} \right)_{A/B}. \quad (7)$$

Interestingly, according to Eqs. (5) and (4), the frequency transfer is completely determined once the expression for the time transfer function is explicitly known (see also Linet and Teyssandier [20], Hees *et al.* [27], Hees *et al.* [28]). Similarly, the time transfer function completely determines the (coordinate) time transfer as seen from Eq. (2).

## B. Analytical expansion of the time transfer function

In the context of atmospheric radio occultation experiments, we are mainly dealing with an optical medium with refractivity (i.e., the quantity defined such that  $N = n - 1$ ) satisfying

$$N(x) \ll 1 \quad (8)$$

everywhere within  $x \in \mathcal{D}$ . This assumption implies that  $\Gamma_{AB}$  is almost a straight line segment joining  $x_A$  to  $x_B$ . According to Bourgoïn *et al.* [23], the time transfer function can thus be decomposed as

$$\mathcal{T}(\mathbf{x}_A, t_B, \mathbf{x}_B) = \frac{\|\mathbf{x}_B - \mathbf{x}_A\|}{c} + \frac{\Delta(\mathbf{x}_A, t_B, \mathbf{x}_B)}{c}, \quad (9)$$

where  $\Delta/c$  is called a delay function [29]. In the present context, the delay function is caused by optical refraction occurring inside  $\mathcal{D}$ . The effect of the optical refraction on the radio signal is twofold as mentioned in Sect. I. First, it changes the phase velocity of the signal creating an excess path delay, and then, it bends the signal trajectory towards regions of higher refractivity generating a geometrical delay. Other delays due to gravitational effects are neglected according to the assumption (1). Therefore, in this paper, the delay function does not account for terms proportional to the gravitational constant  $G$ .

Henceforth, we introduce the parameter  $N_R$  in order to keep track of the degree to which  $\Gamma_{AB}$  deviates from the straight line segment. Let  $N_R$  be the refractivity at a the reference point-event  $x_R$ , that is to say  $N_R = N(x_R)$ . Hereafter, it is convenient to consider that  $x_R$  is the point-event where the value of the measured refractivity is the largest one (e.g., in the case of an occultation by a rocky planet,  $x_R$  would be spatially close to the surface of the planet). Then, we can assume the following linear relationship

$$N(x) = N_R \mathcal{N}(x), \quad (10)$$

where  $\mathcal{N}(x)$  is a scalar function that does not depend on  $N_R$  and which satisfies  $0 < \mathcal{N}(x) \leq 1$ . It follows from Eq. (8) that  $N_R \ll 1$ . In this case, the delay function (and hence the time transfer function) is unique [30] and admits an analytical expansion in ascending power of  $N_R$  :

$$\Delta(\mathbf{x}_A, t_B, \mathbf{x}_B) = \sum_{m=1}^{+\infty} (N_R)^m \Delta^{(m)}(\mathbf{x}_A, t_B, \mathbf{x}_B). \quad (11)$$

Such an expansion is called a post-Minkowskian expansion similarly to what is done with gravity [29]. In that respect, we call  $N_R$  a post-Minkowskian parameter. This terminology is motivated by the so-called optical metric of spacetime whose components are proportional to  $N_R$  (see Eqs. (6) of Bourgoïn *et al.* [23] for the components of the optical metric when the physical metric of spacetime reduces to Minkowski's). Hence, any deviation from the Minkowski spacetime due to refractivity is parameterized by the post-Minkowskian parameter  $N_R$ .

After substituting for  $\Delta$  from Eq. (11) into (9) while applying (4), we find

$$\underline{\mathbf{l}}_A(\mathbf{x}_A, t_B, \mathbf{x}_B) = -\mathbf{N}_{AB} + \sum_{m=1}^{+\infty} (N_R)^m \underline{\mathbf{l}}_A^{(m)}(\mathbf{x}_A, t_B, \mathbf{x}_B), \quad (12a)$$

$$\underline{\mathbf{l}}_B(\mathbf{x}_A, t_B, \mathbf{x}_B) = -\mathbf{N}_{AB} + \sum_{m=1}^{+\infty} (N_R)^m \underline{\mathbf{l}}_B^{(m)}(\mathbf{x}_A, t_B, \mathbf{x}_B), \quad (12b)$$

$$\frac{(k_0)_B}{(k_0)_A} = 1 - \sum_{m=1}^{+\infty} (N_R)^m \frac{\partial}{\partial t_B} \frac{\Delta^{(m)}(\mathbf{x}_A, t_B, \mathbf{x}_B)}{c}, \quad (12c)$$

where  $\mathbf{N}_{AB} = (\mathbf{x}_B - \mathbf{x}_A)/\|\mathbf{x}_B - \mathbf{x}_A\|$  and where we introduce the post-Minkowskian terms  $\underline{\mathbf{l}}_A^{(m)}$  and  $\underline{\mathbf{l}}_B^{(m)}$  such as

$$\underline{\mathbf{l}}_A^{(m)}(\mathbf{x}_A, t_B, \mathbf{x}_B) = \partial_A \Delta^{(m)}(\mathbf{x}_A, t_B, \mathbf{x}_B), \quad (13a)$$

$$\underline{\mathbf{l}}_B^{(m)}(\mathbf{x}_A, t_B, \mathbf{x}_B) = -\partial_B \Delta^{(m)}(\mathbf{x}_A, t_B, \mathbf{x}_B). \quad (13b)$$

Therefore, in order to determine the time and frequency transfers up to the  $m$ th post-Minkowskian order, the expression of the delay function must be known at least up to the same order. The general method to derive the expression of the delay function at the desired post-Minkowskian order is presented in Bourgoïn [19] and is based on previous work by Teyssandier and Le Poncin-Lafitte [29] for the propagation of light rays in a vacuum. The method drastically simplifies when the optical spacetime is stationary.

### C. Stationary and spherical symmetry assumptions

Let us consider that the coordinate system  $(x^\mu)$  is attached to an inertial frame that is centered at the occulting body center-of-mass and is non-rotating with respect to distant stars (see figure 1). In some circumstances the atmospheric properties can be considered stationary within  $(x^\mu)$ , and hence, the optical metric of spacetime is independent of the coordinate time. Thus, the time transfer function and the delay function become independent of  $t_B$  too, so that we can write  $\mathcal{T}(\mathbf{x}_A, \mathbf{x}_B)$  and  $\Delta(\mathbf{x}_A, \mathbf{x}_B)$ , respectively. In addition, the stationarity condition implies that the time component

of the 4-wave covector is a first integral along  $\Gamma_{AB}$  as it might be seen from Eq. (12c), hence  $(k_0)_B - (k_0)_A = 0$ . Accordingly, the expression for the frequency transfer in Eq. (5) reduces to

$$\frac{\nu_B}{\nu_A} = \frac{(u^0)_B}{(u^0)_A} \left( \frac{1 + \boldsymbol{\beta}_B \cdot \underline{\mathbf{l}}_B}{1 + \boldsymbol{\beta}_A \cdot \underline{\mathbf{l}}_A} \right). \quad (14)$$

After substituting for  $\underline{\mathbf{l}}_A$  and  $\underline{\mathbf{l}}_B$  from Eqs. (12) into (14),  $\Delta\nu$ , the frequency shift due to the atmosphere, is given by

$$\Delta\nu = [\nu_B]_{\text{vac}} \left\{ \frac{1 + \sum_{m=1}^{+\infty} (N_R)^m \frac{\underline{\mathbf{l}}_B^{(m)} \cdot \boldsymbol{\beta}_B}{1 - \boldsymbol{\beta}_B \cdot \mathbf{N}_{AB}}}{1 + \sum_{m=1}^{+\infty} (N_R)^m \frac{\underline{\mathbf{l}}_A^{(m)} \cdot \boldsymbol{\beta}_A}{1 - \boldsymbol{\beta}_A \cdot \mathbf{N}_{AB}}} - 1 \right\}, \quad (15)$$

where  $\Delta\nu = \nu_B - [\nu_B]_{\text{vac}}$  with  $[\nu_B]_{\text{vac}}$  being the frequency that would have been received if the light ray were to propagate in a vacuum, that is to say

$$[\nu_B]_{\text{vac}} = \nu_A \frac{(u^0)_B}{(u^0)_A} \left( \frac{1 - \boldsymbol{\beta}_B \cdot \mathbf{N}_{AB}}{1 - \boldsymbol{\beta}_A \cdot \mathbf{N}_{AB}} \right). \quad (16)$$

The deviation from the frequency transfer calculated in a vacuum, namely  $\Delta\nu$ , is thus parameterized by terms proportional to the ascending powers of  $N_R$  that represents the atmospheric contribution.

If we now impose the spherical symmetry assumption, the refractivity, the delay function, and the time transfer function become radial functions. Let  $K$  be the impact parameter of the zeroth-order light path with respect to the center of symmetry (i.e., the center-of-mass of the occulting planet) :

$$K(\mathbf{x}_A, \mathbf{x}_B) = \|\mathbf{N}_{AB} \times \mathbf{x}_A\|. \quad (17)$$

In this context, Eqs. (13) can be alternatively written as

$$\underline{\mathbf{l}}_A^{(m)}(\mathbf{x}_A, \mathbf{x}_B) = -\mathbf{S}_{AB} \times \mathbf{N}_{AB} \left( 1 + \frac{\mathbf{N}_{AB} \cdot \mathbf{x}_A}{R_{AB}} \right) \left[ \frac{\partial \Delta^{(m)}}{\partial K} \right]_{(\mathbf{x}_A, \mathbf{x}_B)}, \quad (18a)$$

$$\underline{\mathbf{l}}_B^{(m)}(\mathbf{x}_A, \mathbf{x}_B) = -\mathbf{S}_{AB} \times \mathbf{N}_{AB} \left( \frac{\mathbf{N}_{AB} \cdot \mathbf{x}_A}{R_{AB}} \right) \left[ \frac{\partial \Delta^{(m)}}{\partial K} \right]_{(\mathbf{x}_A, \mathbf{x}_B)}, \quad (18b)$$

where we introduce  $R_{AB} = \|\mathbf{x}_B - \mathbf{x}_A\|$  and the unit-vector  $\mathbf{S}_{AB}$  such as

$$\mathbf{S}_{AB} = -\frac{\mathbf{N}_{AB} \times \mathbf{x}_A}{\|\mathbf{N}_{AB} \times \mathbf{x}_A\|}. \quad (19)$$

We now wish to determine the expression for  $\Delta^{(m)}$  in the context of an occultation by a spherically symmetric atmosphere. This is the subject of the next section.

#### IV. APPLICATION TO RADIO OCCULTATION EXPERIMENTS

In this section, the main results from Bourgoïn *et al.* [23] are recalled. We focus on the first post-Minkowskian order and systematically neglect higher order terms. In addition, we neglect the light-dragging effect and thus consider that the optical medium is at rest in our coordinate system.

##### A. Modeling of the refractivity profile

Within a spherical neutral atmosphere the refractivity profile can reasonably be modeled such as

$$N(r) = N_R \exp\left(-\frac{r-R}{H}\right) \sum_{m=0}^d b_m r^m, \quad (20)$$

where  $r = \|\mathbf{x}\|$  and  $R = \|\mathbf{x}_R\|$ . In this expression,  $R$  is the radius of reference (i.e. the position where the measured refractivity is the largest one) and  $H$  is the scale height. The polynomial coefficients  $b_m$  are determined for a range of distance (e.g., for  $R \leq r \leq \mathcal{H}$ , with  $\mathcal{H}$  the upper limit of the neutral atmosphere) and shall not be employed outside of these upper and lower limits. In addition, they satisfy the relation  $\sum_{m=0}^d b_m R^m = 1$  at the radius of reference. The degree of the polynomial expansion is denoted by  $d$ .

For most of the known atmospheres within the solar system, the refractivity profile roughly increases exponentially with decreasing altitude which justifies the main exponential trend in Eq. (20). The polynomial factor allows to account for every deviation from the exponential, especially in the upper atmosphere where the exponential variation assumption could be less accurate.

Bourgoin *et al.* [23] have shown that in the spherical symmetry assumption, the delay function can be explicitly determined at the first post-Minkowskian order from the expression (20), in the limit of small velocity of the optical medium. The first order delay function is given here without the light-dragging term :

$$\Delta^{(1)}(K) = \mathcal{L}_K \sum_{m=0}^{+\infty} \frac{(2m-1)!!}{2^m} \left(\frac{H}{K}\right)^m \sum_{n=0}^{m_d} Q_{m-n} B_n(K), \quad (21)$$

with

$$\mathcal{L}_K = \sqrt{2\pi} \sqrt{HK} \exp\left(-\frac{K-R}{H}\right), \quad (22)$$

and

$$m_d = \begin{cases} m & \text{for } m < d, \\ d & \text{for } m \geq d. \end{cases} \quad (23)$$

The non-dimensional coefficient  $B_n$  is defined as

$$B_n(K) = \sum_{l=n}^d \binom{l}{n} b_l K^l, \quad (24)$$

and the coefficient  $Q_m$  is given by

$$Q_m = (-1)^{m+1} \frac{(2m+1) \cdot (2m-3)!!}{2^{2m} \cdot m!}. \quad (25)$$

The binomial coefficient is given by

$$\binom{l}{m} = \frac{l!}{m!(l-m)!}, \quad (26)$$

and the double factorial [31] is defined by

$$m!! = \begin{cases} m \times (m-2) \times \dots \times 3 \times 1 & \text{for } m \text{ odd,} \\ m \times (m-2) \times \dots \times 4 \times 2 & \text{for } m \text{ even,} \\ 1 & \text{for } m = -1, 0, \end{cases} \quad (27a)$$

and

$$(-2m-1)!! = \frac{(-1)^m}{(2m-1)!!} \quad \text{for } m \geq 1. \quad (27b)$$

The expression of the time transfer function is then easily obtained from Eq. (9) and (11).

In the context of radio occultation experiments,  $\phi$ , the bending angle of the light trajectory is an important parameter that can usually be directly linked to the frequency shift. It can be defined from  $\underline{\mathbf{L}}_A$  and  $\underline{\mathbf{L}}_B$  such as

$$\phi(\mathbf{x}_A, \mathbf{x}_B) = \arcsin \left[ \frac{\underline{\mathbf{L}}_A \times \underline{\mathbf{L}}_B}{\|\underline{\mathbf{L}}_A\| \|\underline{\mathbf{L}}_B\|} \cdot \mathbf{S}_{AB} \right]. \quad (28)$$

Therefore, according to Eqs. (12) it is seen that  $\phi$  can be developed in ascending power of  $N_R$ , namely

$$\phi(\mathbf{x}_A, \mathbf{x}_B) = \sum_{m=1}^{+\infty} (N_R)^m \phi^{(m)}(\mathbf{x}_A, \mathbf{x}_B). \quad (29)$$

At first post-Minkowskian order and within spherical symmetry assumption, we had shown from Eqs. (18) that  $\underline{\mathbf{L}}_A$  and  $\underline{\mathbf{L}}_B$  are unit triples. Therefore, the first term of the series expansion of the bending angle is given by

$$\phi^{(1)}(\mathbf{x}_A, \mathbf{x}_B) = - \left[ \frac{\partial \Delta^{(1)}}{\partial K} \right]_{(\mathbf{x}_A, \mathbf{x}_B)}, \quad (30)$$

and can be explicitly determined from (21), that is to say

$$\phi^{(1)}(K) = \frac{\mathcal{L}_K}{H} \sum_{m=0}^{+\infty} \frac{(2m-1)!!}{2^m} \left( \frac{H}{K} \right)^m \sum_{n=0}^{m_d} Q_{m-n} \sum_{l=n}^d \binom{l}{n} b_l K^l \left[ 1 + \frac{H}{K} \left( m - l - \frac{1}{2} \right) \right]. \quad (31)$$

The determination of the uncertainty profiles is based on Eq. (31). However, because uncertainty profiles do not require as much precision as for the direct retrieval of atmospheric properties, the relation can be further simplified assuming, for instance, an isothermal profile which is precisely the subject of the next section.

At first post-Minkowskian order, it is now straightforward to relate the frequency shift residuals to the bending angle. For an application within the solar system, we can always consider that the 3-velocities are small with respect to the speed of light in vacuum, that is to say  $\|\beta_A\|$  and  $\|\beta_B\| \ll 1$ . Thus, at first orders in  $\|\beta_A\|$ ,  $\|\beta_B\|$ , and  $N_R$ , relation (15) simplifies to

$$\frac{\Delta\nu}{[\nu_B]_{\text{vac}}} = N_R \underline{\mathbf{L}}_B^{(1)} \cdot \beta_B - N_R \underline{\mathbf{L}}_A^{(1)} \cdot \beta_A. \quad (32)$$

After substituting for  $\underline{\mathbf{L}}_A^{(1)}$  and  $\underline{\mathbf{L}}_B^{(1)}$  from Eqs. (18) into (32) and after making use of Eqs. (29) and (30), we eventually deduce

$$\left( \frac{\Delta\nu}{[\nu_B]_{\text{vac}}} \right)_K = \phi(K) (\mathbf{S}_{AB} \times \mathbf{N}_{AB}) \cdot \beta_{\text{eff}}, \quad (33)$$

where  $\beta_{\text{eff}}$ , the effective coordinate velocity, is given by

$$\beta_{\text{eff}} = \left( 1 + \frac{\mathbf{N}_{AB} \cdot \mathbf{x}_A}{R_{AB}} \right) \beta_A - \left( \frac{\mathbf{N}_{AB} \cdot \mathbf{x}_A}{R_{AB}} \right) \beta_B. \quad (34)$$

Let us notice that when the receiver is at infinity (e.g., for one-way downlink radio occultations by Titan), the effective velocity reduces to  $\lim_{r_B \rightarrow \infty} \beta_{\text{eff}} = \beta_A$ .

## B. Isothermal assumption and frequency shift

As mentioned before, it is a reasonable approximation, for most of planets or satellites within the solar system, to suppose that their refractivity profile mainly increases exponentially with decreasing altitude which justifies the expression (20). The different factors in this relation can be roughly identified with the pressure and inverse of the temperature by making use of the ideal gas law which returns

$$N(r) = N_R \left( \frac{P}{P_R} \right)_r \left( \frac{T_R}{T} \right)_r, \quad (35)$$

where  $N_R = N_v P_R / (k T_R)$  with  $N_v$  the refractive volume (see e.g., Eshleman [32]) and  $k$  the Boltzmann constant. The pressure and temperature at the level  $r = R$  are denoted by  $P_R = P(R)$  and  $T_R = T(R)$ , respectively.

Ideally, the exponential term in (20) would identify the pressure profile which usually represents the largest contribution to refractivity changes across the altitude. Therefore, it is common to model the pressure profile such as

$$\left( \frac{P}{P_R} \right)_r = \exp \left( -\frac{r-R}{H} \right). \quad (36)$$

And hence, it is seen from (20) that the inverse of the temperature profile would be modeled as

$$\left( \frac{T_R}{T} \right)_r = \sum_{m=0}^d b_m r^m. \quad (37)$$



This interpretation of the different terms in the refractivity works well as long as the pressure profile is indeed a pure exponential. If not, part of the pressure profile is absorbed in the polynomial coefficients, hence they no longer describe the inverse of the temperature profile. In general, this interpretation can work well in the lower part of the atmosphere.

In the context of the determination of uncertainty profiles in atmospheric properties, high accuracy on the physical profiles is not needed. Therefore, the refractivity profile can be simplified such as (see also Withers [15])

$$N(r) = N_R \exp\left(-\frac{r-R}{H}\right), \quad (38)$$

meaning that the only polynomial coefficient  $b_m$  being different from zero in Eq. (20) is  $b_0 = 1$ . In this context, the separation assumed in Eqs. (36) and (37) is a reasonable approximation and Eq. (38) can be roughly interpreted as neglecting the temperature changes before the exponential variations of the pressure inside the atmosphere. Then, at first post-Minkowskian order the delay function due to an isothermal atmosphere reads

$$\Delta(K) = N(K) \sqrt{2\pi} \sqrt{HK} \sum_{m=0}^{+\infty} Q_m \frac{(2m-1)!!}{2^m} \left(\frac{H}{K}\right)^m + \mathcal{O}(N_R^2), \quad (39)$$

and the expression for the bending angle simplifies to

$$\phi(K) = N(K) \sqrt{2\pi} \sqrt{\frac{K}{H}} \sum_{m=0}^{+\infty} Q_m \frac{(2m-1)!!}{2^m} \left(\frac{H}{K}\right)^m \left[1 + \frac{H}{K} \left(m - \frac{1}{2}\right)\right] + \mathcal{O}(N_R^2). \quad (40)$$

Equations (33) and (40) represent the basis of the sensitivity analysis which is developed in the next section.

## V. UNCERTAINTY PROFILES IN ATMOSPHERIC PROPERTIES

In this section, we first derive the uncertainty relationships between the atmospheric properties and the frequency shift residuals. In a second step, we validate our relations with realistic profiles deduced from data of past radio occultation experiments. We use Cassini data for an occultation by Titan, Venus Express (VEX) data for an occultation by Venus, and Mars Global Surveyor (MGS) data for an occultation by Mars.

### A. Uncertainty relationships

From Eq. (33),  $\sigma_\phi$ , the uncertainty in the bending angle, is related to  $\sigma_{\Delta\nu}$ , the uncertainty in the frequency shift, by

$$\sigma_\phi(K) = \frac{\sigma_{\Delta\nu}(K)}{[\nu_B]_{\text{vac}}} |(\mathbf{S}_{AB} \times \mathbf{N}_{AB}) \cdot \boldsymbol{\beta}_{\text{eff}}|^{-1}, \quad (41)$$

where  $|\cdot|$  denotes the absolute value. From Eq. (40),  $\sigma_N$ , the uncertainty in the refractivity, is related to the uncertainty in the bending angle according to

$$\sigma_N(K) = N(K) \frac{\sigma_\phi(K)}{\phi(K)}. \quad (42)$$

This last equation is fundamental for deriving the relationships between the uncertainty in the frequency shift and  $\sigma_T$ ,  $\sigma_P$ , and  $\sigma_\kappa$ , the uncertainties in temperature, pressure, and neutral number density, respectively. The uncertainty in pressure is derived from Eqs. (36) and (38) while the uncertainty in temperature can be determined from the ideal gas law in Eq. (35). The uncertainty in neutral number density is derived from the neutral number density expression, namely  $\kappa(K) = N(K)/N_v$ . We thus obtain the following equations :

$$\sigma_P(K) = P_R \frac{\sigma_N(K)}{N_R}, \quad (43a)$$

$$\sigma_T(K) = T_R \left[1 + \frac{T(K)}{T_R}\right] \frac{\sigma_N(K)}{N(K)}, \quad (43b)$$

$$\sigma_\kappa(K) = \frac{\sigma_N(K)}{N_v}. \quad (43c)$$

While interpreting results from past radio occultation experiments,  $\phi(K)$ ,  $N(K)$ ,  $P(K)$ , and  $T(K)$  should be taken from profiles in atmospheric properties that are determined from the data analysis, for instance, using the Abel inversion method or the ray-tracing technique. However, for performing preliminary design studies of future radio occultation experiments, the profiles can be derived from the theoretical modeling presented in Sect. IV B. Therefore,  $N(K)$  and  $\phi(K)$  can be modeled according to Eqs. (38) and (40), respectively, assuming an a priori knowledge of the atmospheric scale height (see also Withers [15]). The temperature and pressure profiles can be modeled assuming the isothermal hypothesis which leads to  $T(K)/T_R = 1$  and  $P(K)/P_R = N(K)/N_R$ , respectively.

## B. Application to past radio occultation experiments

We now wish to validate our analytical expressions for uncertainties in atmospheric properties by studying results of three representative radio occultation experiments performed at Titan, Mars, and Venus by the Cassini, MGS, and VEX missions, respectively. We consider the three following data set. First, the ingress radio occultation of Cassini by Titan on June 22nd, 2009, recorded by the Deep Space Station (DSS)-14 in one-way X-band link. Secondly, the ingress radio occultation of MGS by Mars on December 27th 1998, recorded by the DSS-25 in one-way X-band link. Finally, the egress radio occultation of VEX by Venus on February 1st, 2014, recorded by the DSS-45 in one-way X-band link. Cassini and MGS data are available on NASA’s Planetary Data System (PDS) (<https://pds.nasa.gov/>). VEX data were provided to us by the Multi-mission "Planetary Radar and Radio Sciences Group" at Jet Propulsion Laboratory (JPL), California Institute of Technology.

Owing to the fact that the three atmospheres are stationary and spherically symmetric to a good extend, the refractivity is derived by invoking the Abel inversion method. The frequency shift is modeled from the ephemerides of the spacecraft and planets, and these are given by NASA’s SPICE toolkit Navigation and Ancillary Information Facility (NAIF) [33]. Then, the physical properties (e.g., the neutral number density, the pressure, and the temperature) can be inferred by making use of the ideal gas law together with hydrostatic equilibrium assumption (see e.g., Schinder *et al.* [9] for Titan, Fjeldbo and Eshleman [5] for Mars, and Fjeldbo *et al.* [14], Gramigna *et al.* [34] for Venus). Therefore, the profiles  $\phi(K)$ ,  $N(K)$ ,  $P(K)$ , and  $T(K)$  that are needed for evaluating our analytical solutions in Eqs. (41), (42), and (43) are determined from the data processing and are depicted as plain black curves labeled “Abel inv.” in figures 3, 4, and 5 for Venus, Titan, and Mars, respectively. These profiles have been validated by comparing them to those published in the literature (see an example with Titan’s temperature profile in figure 2). The atmospheric profiles for Titan and Mars are derived up to the surface of the bodies, so that  $R$ , the altitude of reference, is given by the equatorial radius. For Venus, however, the profiles cannot be computed below 45 km altitude due to low value of the signal to noise ratio. Therefore, the altitude of reference in this case is taken 45 km above the surface.

Hereafter, our analytical uncertainties are compared to reference uncertainties that are obtained from a Monte Carlo simulations [17]. The methodology to derive Monte Carlo estimates proceeds as follows. First, a random Gaussian noise is added to the original time-series of the frequency residuals. The Allan deviation of the noise is fixed to  $\sigma_{\Delta\nu}$ , the noise of the frequency residuals outside the atmosphere. Secondly, 2000 (adding more profiles does not significantly change the results) independent determinations of atmospheric properties are performed using the Abel inversion method, each time for a different realization of the random noise. In addition, the boundary temperature at the top of the neutral atmosphere is randomly chosen with a  $\pm 40$  K uncertainty range since the computation of the temperature and pressure profile requires an *a priori* guess of the initial value of the temperature (see e.g., discussion in Eshleman [32]). Finally, the standard deviations of the bending angle, the neutral number density, the temperature, and the pressure profiles are assessed. These uncertainty profiles of reference are depicted as black dots labeled “sd(MC)” in figures 3, 4, and 5, for Venus, Titan, and Mars, respectively.

By invoking Eqs. (41), (42), and (43), we determine the predicted uncertainties in atmospheric properties by making use of the computed profiles  $\phi(K)$ ,  $N(K)$ ,  $P(K)$ , and  $T(K)$ . These analytical estimates are depicted as plain red curves labeled “sd(ana)” in figures 3, 4, and 5, for Venus, Titan, and Mars, respectively. Our results are compared to the uncertainty predictions by Withers [15, 16]. Results by Withers are depicted as blue dashed curves and blue dash-dotted curves labeled “Whiters (2010)” and “Whiters (2020)”, respectively. Let us emphasize that Withers only provides  $\sigma_n$ , the neutral number density uncertainty. So, we used relations (41), (42), and (43) in order to infer Withers’ uncertainty predictions for the bending angle, pressure, and temperature profiles, even if these quantities were not provided in the original Withers’ papers.

From a general point of view, our analytical predictions in Eqs. (41), (42), and (43) show really good agreement with respect to the reference uncertainty profiles inferred from the Monte Carlo simulations. The largest differences are observed for the dense atmosphere of Venus (cf., figure 3). For instance, around 45 km altitude the predicted analytical uncertainty is  $\pm 0.31$  Pa for the pressure whereas the Monte Carlo simulations return a value of  $\pm 2.5$  Pa (we report in table I, the profile values at the surface for Titan and Mars, and the profile values at 45 km for Venus). Therefore, for dense neutral atmospheres such as Venus, the first order analytical expressions provide slightly optimistic uncertainties,

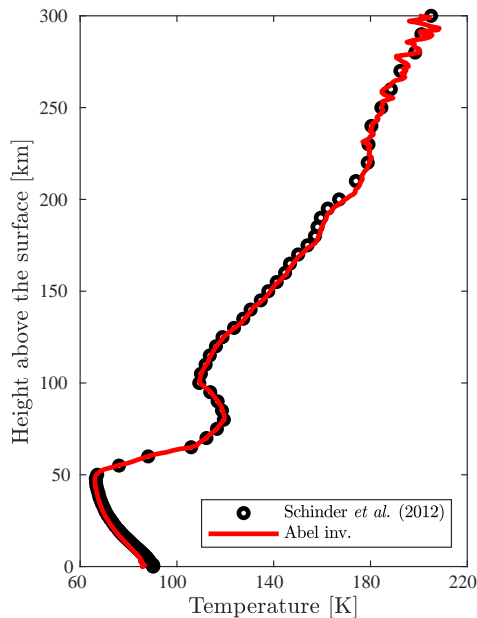


FIGURE 2. Temperature profile in Titan’s atmosphere deduced from the occultation of Cassini on June 22nd, 2009. The red curve is determined from our own Abel inversion software. The black dots represent the temperature profile published in Schinder *et al.* [9] for the same occultation.

up to a factor 8.3 in the pressure profile (cf. table I). For the neutral number density the analytical uncertainty is also optimistic by a factor 6.3, and the most plausible explanation is that the analytical estimates were determined at first order in  $N_R$  (cf., Sect. IV) while second order terms might become important to account for, when dealing with low altitudes within dense atmospheres. Concerning the offsets in the temperature and pressure profiles (cf. figure 3), they could be due to the isothermal hypothesis which is potentially too restrictive in the present context. We note that both analytical methods proposed by Withers cannot exactly replicate the Monte Carlo uncertainty profiles in Venus’ atmosphere, too, due to similar approximations. We note, however, that the analytical uncertainty in the bending angle is in really good agreement with Monte Carlo simulations since they only differ by one part in  $10^2$ . This is due to the fact that the bending is directly related to the frequency shift residuals (according to Eq. (33)) and is independent of the isothermal assumption.

For the cases of Titan and Mars, the agreement between the analytical uncertainty profiles and Monte Carlo’s is excellent (cf., figures 4 and 5, respectively). At Titan’s surface, the least accurate prediction is the uncertainty in the pressure profile which is optimistic by a factor of 3.7, only. At Mars’ surface, the least accurate prediction is the uncertainty in the neutral number density which is conservative up to a factor of 2.8. For the three cases presented here (Venus, Titan, and Mars), let us emphasize that the analytical estimates always succeed in reproducing the general trend of the Monte Carlo uncertainties. This is also true for Venus’ temperature and pressure profiles, even though the analytical predictions are shifted with respect to the Monte Carlo’s ones. Finally, let us mention that our analytical estimates are consistent, most of the time, with the ones derived by Withers [15]. The origin of this behavior becomes clear when relation (40) is compared to Eq. (35) of Withers [15]. The difference between the two expressions, that were derived using two different frameworks, is in the order of  $H/K$  which is small in general. However, our analytical uncertainties, especially in temperature and pressure, remain closer to the Monte Carlo estimates than Withers’ predictions. This is particularly visible for cases of Titan and Mars.

## VI. CONCLUSIONS

In this work, we present new relationships for finding the uncertainties in neutral atmosphere properties measured by radio occultation experiments. Our approach is based on results of previous works (see Bourgoïn [19], Bourgoïn *et al.* [23]) that aimed at determining the time and frequency transfers to a high degree of precision when the electromagnetic signal is crossing a neutral medium. By considering the first order solutions of Bourgoïn *et al.* [23], we are able to derive analytical expressions describing the evolution of the delay function and the bending angle during an occultation by a stationary and spherically symmetric atmosphere. The delay function and the bending

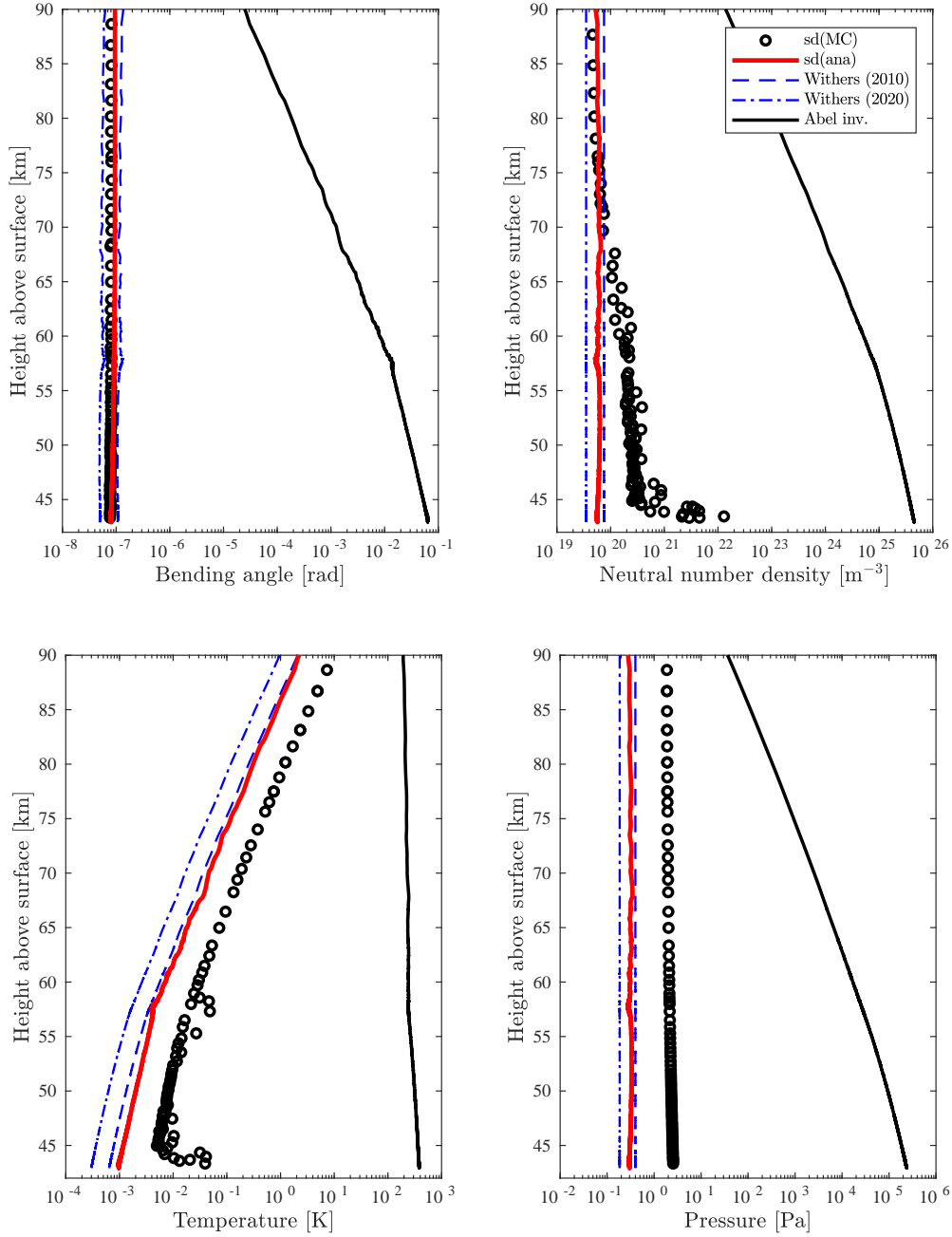


FIGURE 3. Uncertainties in bending angle (upper left panel), neutral number density (upper right panel), temperature (lower left panel), and pressure (lower right panel) for the VEX-Venus occultation. The plain black curve represents the physical profile obtained from the Abel inversion method. The black dots represent the Monte Carlo reference uncertainties, the red curve shows our analytic isothermal uncertainty obtained from Eqs. (41) and (43) and the blue dashed line and the dashed-dotted line represent the curves obtained from Withers [15] and Withers [16], respectively.

angle are needed to determine explicit expressions for the time and frequency transfers. Noticing that, in general, the refractivity profile is dominated by pressure variations before temperature changes across the profile, we simplify the relationships assuming an isothermal atmosphere. We thus provide simplified equations (cf., Eqs. (39) and (40)) that are then used as starting points for deriving uncertainty relationships. The uncertainty relationships allow to relate the errors in the frequency shift to those in the bending angle, the refractivity, the neutral number density, the temperature, or the pressure. The relationships are given explicitly in Eqs. (41), (42), and (43). We validate these from results of past radio occultation experiments performed at Titan, Mars, and Venus by the Cassini, MGS, and VEX missions, respectively. We thus perform Monte Carlo simulations in order to assess uncertainty relationships

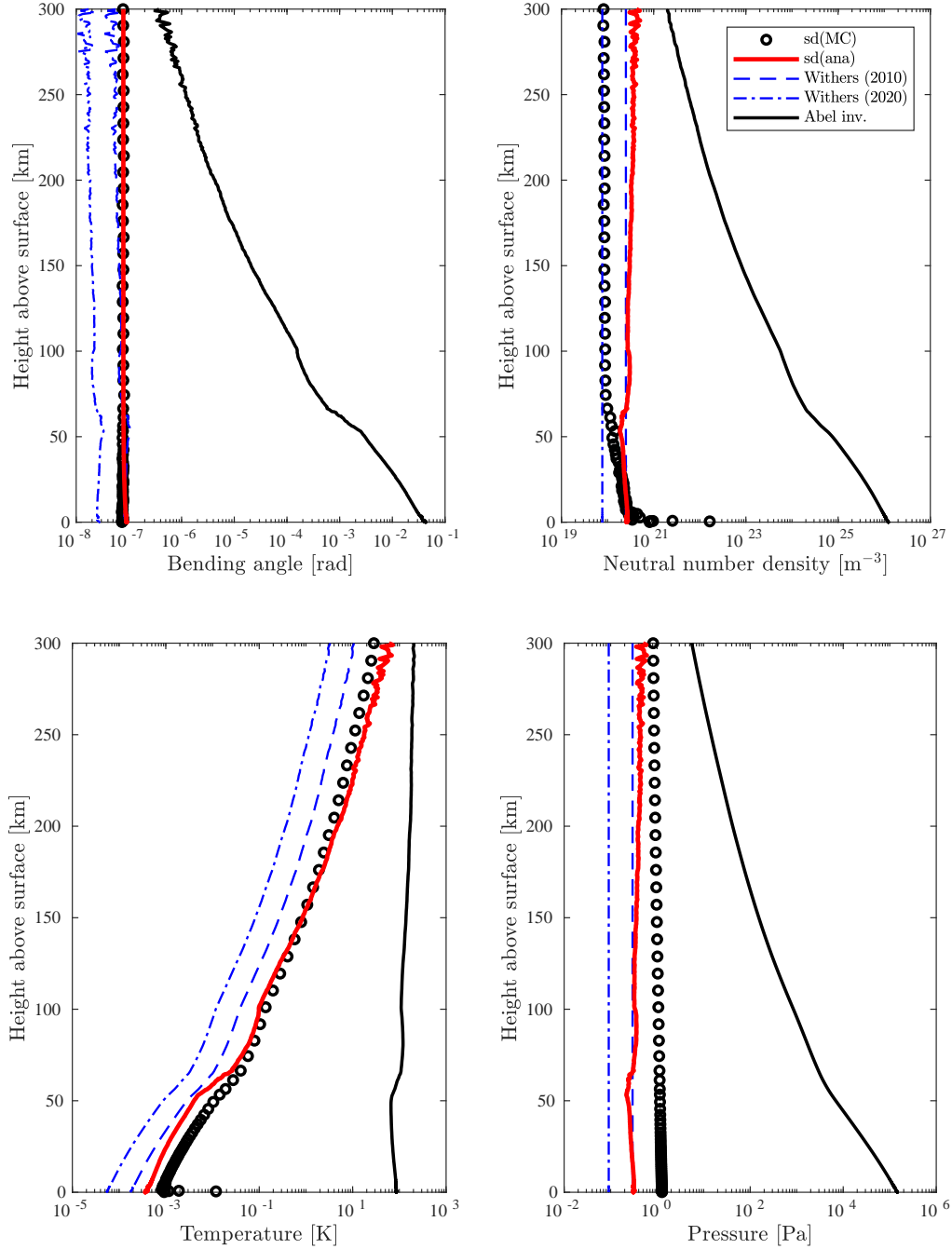


FIGURE 4. Uncertainties in the bending angle (upper left panel), neutral number density (upper right panel), temperature (lower left panel), and pressure (lower right panel) for the Cassini-Titan occultation. See caption of figure 3 for additional details.

that are then compared to the analytical predictions in Eqs. (41), (42), and (43). The analytical estimates prove to replicate very accurately the numerical results from the Monte Carlo simulations. For the case of dense atmospheres, such as Venus, although the analytical error profiles can be optimistic, they nevertheless capture well the trend of the uncertainty profiles (see figure 3). Concerning the case of more tenuous atmospheres, such as the ones of Titan and Mars, the analytical uncertainties are in really good agreement with Monte Carlo simulations (see figures 4 and 5). In addition, for certain quantities such as the neutral number density or the temperature, the analytical predictions are similar to Withers' [15] especially at low altitudes. Withers [15] provides uncertainty for the neutral number density only, so we used our relationships to extrapolate his results for the temperature, pressure and bending angle. Our method, by providing uncertainties also for temperature and pressure, is thus complementary to Withers [15, 16].

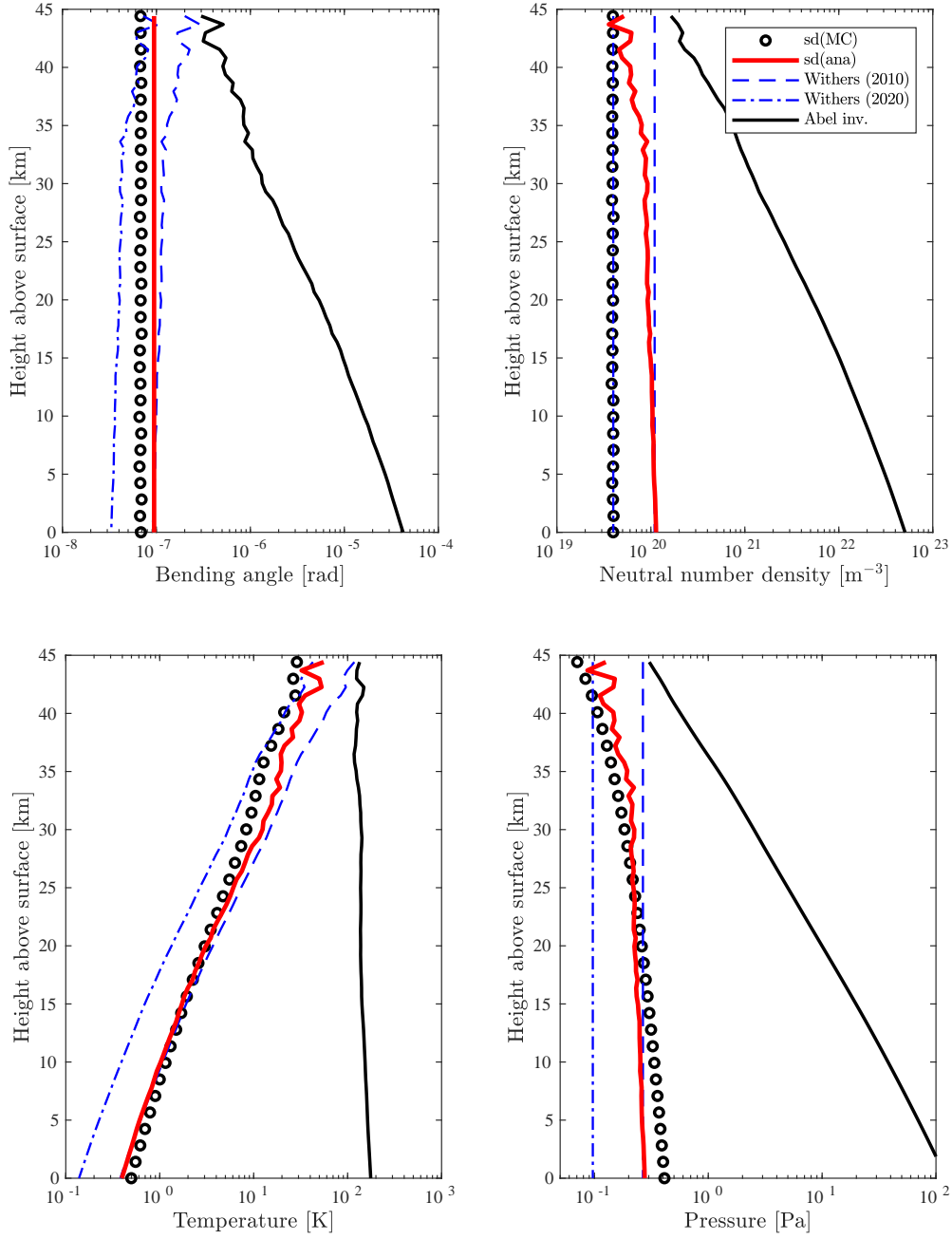


FIGURE 5. Uncertainties in the bending angle (upper left panel), neutral number density (upper right panel), temperature (lower left panel), and pressure (lower right panel) for the MGS-Mars occultation. See caption of figure 4 for additional details.

However, Withers' methods consider the characteristics of the experiment outside the atmosphere only to retrieve uncertainties. Conversely, our method, instead, allows to obtain higher accuracy uncertainty profiles since it depends on the characteristics of the experiment and its variations along the whole atmosphere. In addition, the complete experiment occultation geometry is taken into account as a function of the altitude.

Lastly, the uncertainty relationships derived in Eqs. (41), (42), and (43), are particularly useful for interpreting results of past radio occultation experiments. In this attempt, the different atmospheric properties  $\phi(K)$ ,  $N(K)$ ,  $P(K)$ , and  $T(K)$ , that are needed for the computation, should be taken from results of the data analysis, for instance, using the Abel inversion method or the ray-tracing technique. However, uncertainty relationships can also be employed for performing preliminary design studies of future radio occultation experiments. In that case, the profiles can be derived from theoretical modelings presented in Sect. IV B. As for Withers [15], an a priori knowledge of the scale height is needed.

TABLE I. Table of errors for the bending, the neutral number density, the temperature, and the pressure. Values for Venus are given at 45 km.

Profiles		Titan	Mars	Venus
$\phi$ [rad]	Abel	$4.3 \times 10^{-2}$	$4.2 \times 10^{-5}$	$6.4 \times 10^{-2}$
	sd(ana)	$9.1 \times 10^{-8}$	$9.5 \times 10^{-8}$	$8.0 \times 10^{-8}$
	sd(MC)	$7.7 \times 10^{-8}$	$6.9 \times 10^{-8}$	$7.8 \times 10^{-8}$
$\kappa$ [m <sup>-3</sup> ]	Abel	$1.2 \times 10^{26}$	$5.1 \times 10^{22}$	$3.7 \times 10^{25}$
	sd(ana)	$2.6 \times 10^{20}$	$1.1 \times 10^{20}$	$5.6 \times 10^{19}$
	sd(MC)	$3.4 \times 10^{20}$	$4.0 \times 10^{19}$	$3.5 \times 10^{20}$
$T$ [K]	Abel	85.8	176.1	362.5
	sd(ana)	$3.7 \times 10^{-4}$	$3.9 \times 10^{-1}$	$9.8 \times 10^{-4}$
	sd(MC)	$6.7 \times 10^{-4}$	$5.0 \times 10^{-1}$	$4.2 \times 10^{-3}$
$P$ [Pa]	Abel	$1.5 \times 10^5$	$1.2 \times 10^2$	$1.8 \times 10^5$
	sd(ana)	$3.1 \times 10^{-1}$	$2.8 \times 10^{-1}$	$3.1 \times 10^{-1}$
	sd(MC)	1.1	$4.1 \times 10^{-1}$	2.5

To conclude, our method could be further improved by releasing the isothermal assumption and considering the full solutions of Sect. IV A. In addition, a more complete solution could be considered including higher order terms in  $N_R$  or considering the relativistic light-dragging effect which was derived in Bourgoïn *et al.* [23].

## VII. ACKNOWLEDGMENTS

The authors are grateful to Dustin Buccino and Kamal Oudrhiri from the Multi-mission "Planetary Radar and Radio Sciences Group" at Jet Propulsion Laboratory (JPL), California Institute of Technology, for providing the Venus Express radio occultation data used in this paper. The authors are also thankful to Andrea Caruso for providing simulated data for testing our Monte-Carlo simulations. The authors are grateful to the Italian Space Agency (ASI) for financial support through Agreement No. 2018-25-HH.O in the context of ESA's JUICE mission, and Agreement No. 2020-13-HH.O in the context of TRIDENT's mission Phase A study. A.B. is grateful to Centre National d'Études Spatiales (CNES) for financial support.

- 
- [1] F. Roques, B. Sicardy, R. G. French, W. B. Hubbard, A. Barucci, P. Bouchet, A. Brahic, J.-A. Gehrels, T. Gehrels, I. Grenier, T. Le Bertre, J. Lecacheux, J. P. Maillard, R. A. McLaren, C. Perrier, F. Vilas, and M. D. Waterworth, *A&A* **288**, 985 (1994).
- [2] B. Sicardy, F. Colas, T. Widemann, A. Bellucci, W. Beisker, M. Kretlow, F. Ferri, S. Lacour, J. Lecacheux, E. Lellouch, S. Pau, S. Renner, F. Roques, A. Fienga, C. Etienne, C. Martinez, I. S. Glass, D. Baba, T. Nagayama, T. Nagata, S. Itting-Enke, K.-L. Bath, H.-J. Bode, F. Bode, H. Lüdemann, J. Lüdemann, D. Neubauer, A. Tegtmeier, C. Tegtmeier, B. Thomé, F. Hund, C. deWitt, B. Fraser, A. Jansen, T. Jones, P. Schoenau, C. Turk, P. Meintjies, M. Hernandez, D. Fiel, E. Frappa, A. Peyrot, J. P. Teng, M. Vignand, G. Hesler, T. Payet, R. R. Howell, M. Kidger, J. L. Ortiz, O. Naranjo, P. Rosenzweig, and M. Rapaport, *Journal of Geophysical Research (Planets)* **111**, E11S91 (2006).
- [3] A. Kliore, D. L. Cain, G. S. Levy, V. R. Eshleman, G. Fjeldbo, and F. D. Drake, *Science* **149**, 1243 (1965).
- [4] G. Fjeldbo and V. R. Eshleman, *J. Geophys. Res.* **70**, 3217 (1965).
- [5] G. Fjeldbo and V. R. Eshleman, *Planet. Space Sci.* **16**, 1035 (1968).
- [6] G. F. Lindal, D. N. Sweetnam, and V. R. Eshleman, *AJ* **90**, 1136 (1985).
- [7] G. F. Lindal, J. R. Lyons, D. N. Sweetnam, V. R. Eshleman, and D. P. Hinson, *J. Geophys. Res.* **92**, 14987 (1987).
- [8] G. F. Lindal, *AJ* **103**, 967 (1992).
- [9] P. J. Schinder, F. M. Flasar, E. A. Marouf, R. G. French, C. A. McGhee, A. J. Kliore, N. J. Rappaport, E. Barbini, D. Fleischman, and A. Anabtawi, *Icarus* **221**, 1020 (2012).
- [10] P. J. Schinder, F. M. Flasar, E. A. Marouf, R. G. French, A. Anabtawi, E. Barbini, and A. J. Kliore, *Radio Science* **50**, 712 (2015).
- [11] A. K. Steiner, G. Kirchengast, and H. P. Ladreiter, *Annales Geophysicae* **17**, 122 (1999).
- [12] R. A. Anthes, P. A. Bernhardt, Y. Chen, L. Cucurull, K. F. Dymond, D. Ector, S. B. Healy, S. P. Ho, D. C. Hunt, Y. H. Kuo, H. Liu, K. Manning, C. McCormick, T. K. Meehan, W. J. Randel, C. Rocken, W. S. Schreiner, S. V. Sokolovskiy,

- S. Syndergaard, D. C. Thompson, K. E. Trenberth, T. K. Wee, N. L. Yen, and Z. Zeng, *Bulletin of the American Meteorological Society* **89**, 313 (2008).
- [13] R. A. Phinney and D. L. Anderson, *J. Geophys. Res.* **73**, 1819 (1968).
- [14] G. Fjeldbo, A. J. Kliore, and V. R. Eshleman, *AJ* **76**, 123 (1971).
- [15] P. Withers, *Advances in Space Research* **46**, 58 (2010).
- [16] P. Withers, *Advances in Space Research* **66**, 2466 (2020).
- [17] P. J. Schinder, F. M. Flasar, E. A. Marouf, R. G. French, C. A. McGhee, A. J. Kliore, N. J. Rappaport, E. Barbinis, D. Fleischman, and A. Anabtawi, *Icarus* **215**, 460 (2011).
- [18] B. Lipa and G. L. Tyler, *Icarus* **39**, 192 (1979).
- [19] A. Bourgoïn, *Phys. Rev. D* **101**, 064035 (2020).
- [20] B. Linet and P. Teyssandier, *Phys. Rev. D* **66**, 024045 (2002).
- [21] C. Le Poncin-Lafitte, B. Linet, and P. Teyssandier, *Classical and Quantum Gravity* **21**, 4463 (2004), arXiv:gr-qc/0403094.
- [22] W. Gordon, *Annalen der Physik* **377**, 421 (1923).
- [23] A. Bourgoïn, M. Zannoni, L. Gomez Casajus, P. Tortora, and P. Teyssandier, *A&A* **648**, A46 (2021), arXiv:2012.15768 [gr-qc].
- [24] A. Bourgoïn, M. Zannoni, and P. Tortora, *A&A* **624**, A41 (2019), arXiv:1901.08461 [physics.class-ph].
- [25] J. L. Synge, *Relativity: The General Theory* (North-Holland Publ. Co., Amsterdam, 1960).
- [26] L. Blanchet, C. Salomon, P. Teyssandier, and P. Wolf, *Astronomy and Astrophysics* **370**, 320 (2001).
- [27] A. Hees, B. Lamine, S. Reynaud, M.-T. Jaekel, C. Le Poncin-Lafitte, V. Lainey, A. Füzfa, J.-M. Courty, V. Dehant, and P. Wolf, *Classical and Quantum Gravity* **29**, 235027 (2012).
- [28] A. Hees, S. Bertone, and C. Le Poncin-Lafitte, *Phys. Rev. D* **89**, 064045 (2014).
- [29] P. Teyssandier and C. Le Poncin-Lafitte, *Classical and Quantum Gravity* **25**, 145020 (2008), arXiv:0803.0277.
- [30] B. Linet and P. Teyssandier, *Phys. Rev. D* **93**, 044028 (2016).
- [31] G. Arfken, *Mathematical Methods for Physicists*, 3rd ed. (Academic Press, Inc., San Diego, 1985).
- [32] V. R. Eshleman, *Planet. Space Sci.* **21**, 1521 (1973).
- [33] C. H. Acton, *Planet. Space Sci.* **44**, 65 (1996).
- [34] E. Gramigna, M. Parisi, D. Buccino, L. Gomez Casajus, M. Zannoni, P. Tortora, and K. Oudrhiri, arXiv e-prints , arXiv :2102.08300 (2021), arXiv:2102.08300 [astro-ph.EP].